

NUCLEATE BOILING IN LONG-TERM CRYOGENIC PROPELLANT STORAGE IN MICROGRAVITY

Cyrill B. Muratov*

Department of Mathematical Sciences, New Jersey Institute of Technology, Newark, NJ 07102, USA
muratov@njit.edu

V. V. Osipov*, V. N. Smelyanskiy*, R. W. Tyson†

Efficient storage of cryogenic propellants in zero-gravity or microgravity environments is one of the key requirements to enable new long-range space exploration missions currently envisioned by NASA. Recent advances in multi-layer insulation (MLI) allow to sharply reduce the heat leak into cryogenic propellant storage tanks through the tank surface and, as a consequence, significantly extend the storage duration. In this situation the MLI penetrations, such as support struts, feed lines, etc., become significant challenges of the tank's heat management. This problem is especially acute for liquid hydrogen (LH₂) storage, since currently no efficient cryocoolers exist that operate at very low LH₂ temperatures (~20K). In the absence of active cooling the heat leaks through the MLI penetrations will inevitably cause the onset of localized boiling at the tank walls. Our estimates show that for realistic values of local heat inflow the rate by which vapor bubbles are generated near the penetrations will exceed by one or several orders of magnitude the rate of bubble collapse in the subcooled liquid. Therefore, with time vapor bubbles may accumulate within the liquid and drift towards the stagnation areas of the liquid flow in the presence of mixers. Thus, even small heat leaks under microgravity conditions and over the period of many months may give rise to a complex slowly-developing, large-scale spatiotemporal physical phenomena in a multi-phase liquid-vapor mixture. These phenomena are not well-understood nor can be easily controlled. They can be of a potentially hazardous nature for long-term on-orbital cryogenic storage, propellant loading, tank chilldown, engine restart, and other in-space cryogenic fluid management operations. We performed some basic physical estimates to evaluate the relative importance of different physical processes during long-term cryogenic storage of LH₂. Our main goal was to identify the processes and issues, such as safety hazards and design optimization parameters, which arise specifically during extended periods in zero- and microgravity. The next step in developing a better physical understanding of long-term cryogenic storage systems and finding new engineering design solutions is to obtain new fundamental data from on-orbit cryogenic storage experiments. We propose a conceptual design for an ISS-based medium-scale cryogenic storage tank experiment that would probe vapor bubble formation, growth, motion, coalescence and collapse in the presence of localized heat sources in a microgravity environment in the presence of stirring jets of different configurations and passive cooling devices such as MLI, thermodynamic vent system, and vapor-cooled shield.

I Introduction

This paper aims at discussing some of the basic physics issues associated with long-term storage of cryogenic liquids in zero gravity or microgravity environments. By "long-term" we mean, for example, the durations of the currently envisioned extended storage periods in the low earth orbit (LEO), which range from months to years. For NASA's present and future space exploration missions, understanding the behavior of cryogenic liquids over long periods of storage is of crucial importance, because of the fundamental role played by cryogenic propellants, primarily liquid hydrogen (LH₂) and liquid oxygen (LOX), in rocket propulsion, specifically for long-range missions [1]. The very feasibility of using liquid propellant engines

based on LH₂ and LOX in the future long-range missions depends on the success of storing these propellants under microgravity or zero gravity for extended periods of time. One of the currently considered exploration strategies calls for the development of propellant storage and transfer facilities in LEO [2]. These "fuel depots" will need to be able to spend significant amounts of time (at least on the order of several months) in LEO without any substantial propellant losses due to boil-off [2–5]. With the current passive heat insulation technologies, it is theoretically possible to reduce the cryogen boil-off rate to below 3% per month [6]. Even so, this issue becomes a challenge when the required storage duration exceeds 6 months, and yet a greater one for manned missions to Mars [7].

Cryogenic fluid management (CFM) in microgravity provides a number of fundamental physical challenges, many of which were previously discussed in the literature [6, 8–13]. This is especially relevant to storage of LH₂ because of its low critical temperature. One of the main features of microgravity environments is that due to

*Applied Physics Group, Intelligent Systems Division, NASA Ames Research Center Moffett Field, CA 94035-1000, USA, viatcheslav.v.osipov@nasa.gov, vadim.n.smelyanskiy@nasa.gov

†Center for System Studies, University of Alabama Huntsville, 301 Sparkman Drive, Huntsville, AL 35899, USA, richard.w.tyson@nasa.gov

much-reduced levels of g -forces and their generally time-varying character, the vapor bubbles that form as a result of boil-off at the tank walls mainly near MLI penetrations (hot-spots) will not rise quickly towards the ullage space, as they do under normal gravity. Instead, they may slowly grow to very large sizes (tens of centimeters), or they may detach from the wall, migrate toward the stagnation areas of the stirring flow and accumulate there, forming regions of saturated liquid and complicated foam-like vapor-liquid structures whose properties may be not easy to control. These processes are governed by the complex heat transfer mechanisms in the near-wall region; capillary and g -forces; complex dynamics of nucleate boiling; bubble growth, detachment and collapse; chemical traces that can accumulate in the liquid with time and affect its properties. In long-term storage missions foam or bubble colonies can grow at the expense of the single ullage space. They may not be easily removed by tank pressurization because the heat released from vapor condensation may raise the temperature of the liquid surrounding the bubbles to the saturation temperature at the higher pressure. Capillary forces may be sufficiently strong to prevent the detachment of the foam from the tank walls by any realistic stirring flow that keeps the ullage intact. Basic challenges, therefore, include control of the tank pressure, temperature, ullage space size and location, boil-off venting, and work of liquid acquisition devices (LAD) that can be clogged by the foam. Similarly, since the role of buoyancy-driven convection, which is the main mechanism of heat transfer on earth, is greatly reduced in microgravity, heat transfer mechanisms will be significantly altered. Vapor and fluid motion, in turn, will be dominated by the capillary forces, heat transfer-mediated bubble dynamics, bubble coalescence and the induced thermocapillary convection. The resulting bubble patterns and near-wall dynamics, especially around the MLI penetrations can substantially depend on the type of the wall material, chemical traces, vibrations and other external factors.

In view of these complications, the basic technical issues that need to be dealt with in today's design of successful cryogenic storage and transfer devices for long-term operation in microgravity: heat transfer management, pressure control, design of tank stirring, mass gauging, liquid acquisition, and fluid transfer are much more challenging [11], compared to the Apollo era short duration missions, in which a low level of gravity was propulsively maintained [14–16].

A successful treatment of the pressing technical issues of cryogen management in microgravity is impossible without a thorough mechanistic understanding of the underlying physical processes of nucleate boiling. Surprisingly, detailed physical understanding of nucleate boiling phenomena is still lacking today (see e.g. [17]). This may be due to the fact that boiling is a strongly non-

equilibrium phenomenon in which an interplay between stochastic nucleation events at the micro-scale and complicated deterministic nonlinear dynamics at macro-scale takes place (for reviews, see [18–20]). At the same time, since microgravity presents quite a different environment compared to the usual environment on earth, one should exercise caution in applying the engineering correlations developed under earth gravity conditions to the design of cryogenic systems to be operated in space [20, 21]. To address the above technology gaps, it is necessary to collect fundamental data on liquid-vapor structure and dynamics during long-term storage in microgravity from carefully designed in-space long-duration experiments. Experimental work should be done in combination with a detailed physics analysis, mechanistic modeling, first principles computational and multi-scale approaches.

Here we perform some basic physical estimates in order to evaluate the relative importance of different physical processes during long-term cryogenic storage. We concentrate our efforts on LH₂, since it is the cryogen of primary importance to rocket propulsion and is also the most difficult in terms of CFM due to its low boiling point. Let us emphasize that we aim at obtaining only relatively rough estimates that take into account the *long-term* nature of storage. Thus, our main tool will be dimensional analysis, with minimal reference to more advanced mathematical tools. Once the main physical processes acting on the considered long timescales are identified, relevant space experiments can be designed and more precise calculations may be made using advanced mathematical and high-fidelity computational tools. In short, our main goal is to identify these processes and the issues, such as safety hazards and design optimization parameters, which arise specifically during extended periods in microgravity.

II Background

We start with some basic considerations relevant to large-scale cryogenic storage in microgravity. To fix ideas, let us consider one of the proposed designs for the LH₂ tank of the Earth Departure Stage (EDS) for moon missions [22], in which the tank has the shape of a rounded cylinder with height $H_0 = 12$ m and radius $R_0 = 2.5$ m, containing 15 tons of LH₂. The scale of the tank is similar to that used in the S-IVB stage of the Saturn V rocket in the 1960's and 70's, and a brief comparison is, therefore, appropriate.

Indeed, NASA's most comprehensive experience with large-scale cryogenic storage tanks in orbital conditions goes back to the Apollo moon missions¹ [15, 16, 24]

¹We note that liquid helium (LHe) has flown for extended periods of time on a number of scientific missions [13]. Let us point out, however, that in these missions LHe is chilled down to the superfluid state. This makes the case of LHe storage very different from all other cryo-

(see also reviews of other CFM experimental activities in [9, 14]). The third stage of the Saturn V rocket was propelled by LH₂ and LOX, 19,800 kg and 88,800 kg, respectively (here and below the numbers are from the Apollo 17 mission [25, 26]). About a quarter of the propellants (5,000 kg of LH₂ and 25,200 kg of LOX) was utilized for orbital insertion, and the remaining amount was used for the translunar injection burn. Once in orbit, the third stage spent about 3 hours in LEO. The tank insulation (polyurethane foam attached to the tank interior wall) brought the LH₂ boil-off amount down to about 1,000 kg, still an acceptable margin of under 10% of LH₂ available for the second burn. The flow of continuously vented hydrogen vapor (GH₂) was used to provide enough thrust (on the order of $10^{-5}g - 10^{-4}g$) to ensure that the propellants were settled at the bottoms of the tanks at all times during the orbital coast phase. The presence of small upward g -force ensured that the boil-off bubbles rose in the thin convective layer along the tank walls without entering the bulk liquid. Immediately prior to the second burn, the LH₂ tank was rapidly pressurized by the stored heated helium gas (GHe), raising the tank pressure from about 1.5 to 2 atm. This short-time pressurization, followed by firing of the ullage motors must have condensed the smaller vapor bubbles and made the larger bubbles move towards the ullage. The resulting LH₂ liquid at the bottom of the tank should have, therefore, contained little or no bubbles, allowing to safely fire the engine. After that, the thrust of the engine maintained the gas-free liquid at the LH₂ intake, with screens adding an extra protection.

While hugely successful in bringing man to the surface of the moon and back, this approach may not be applied to the missions currently under consideration. The key reason why the Apollo CFM approach worked for the lunar program was that the required in-orbit storage time for the cryogenic propellants was short enough, so it was possible to tolerate a large boil-off rate and, as a consequence, avoid microgravity conditions altogether during the time in orbit. Thus, the Apollo approach carefully avoided dealing with long-term CFM issues associated with microgravity. Any kind of large modern long-range mission, however, would require storing cryogens for extended periods of time. To achieve this, one would need to drastically reduce the amount of boil-off and work in micro- g or zero- g environments. New approaches are, therefore, needed to answer these emerging challenges.

Modern multi-layer insulation (MLI) allows to dramatically reduce the boil-off rate compared to the Apollo missions. Let us assume that the tank is wrapped in an MLI blanket of 50 layers. Using the Lockheed correlation [27], we can estimate the heat flux through the MLI,

gens, since, in contrast to all other cryogens, superfluid LHe has infinite heat conductivity [23], which prevents it from thermal stratification and nucleate boiling.

given the outer environment temperature $T_0 \simeq 240\text{K}$, to be $q_0 \simeq 7.4 \times 10^{-2} \text{ W/m}^2$ [28]. Taking for simplicity the tank area to be $S_0 = 2\pi R_0 H_0 \simeq 200\text{m}^2$, we obtain a lower bound of $Q_0 = q_0 S_0 \simeq 15 \text{ W}$ for the total heat flow into the tank, with the corresponding boil-off rate of at least 90 kg/month, or 0.6% of the propellant mass per month. Of course, these numbers must underestimate the actual heat flow, since they do not take into account heat leaks through various MLI penetrations by struts, feed lines, etc., as well as imperfections in the MLI itself. Let us also note that the heat flux depends very sensitively on the outer environment temperature T_0 . In the extreme case of $T_0 \simeq 400\text{K}$, we find $q_0 \simeq 0.8 \text{ W/m}^2$, an order of magnitude higher than the one computed previously, resulting in the heat flow of $Q_0 \simeq 160 \text{ W}$ and an unacceptably high boil-off rate of 6% per month.

Even with very efficient MLI insulation, the loss of propellant becomes prohibitive for extended missions. Therefore, active boil-off reduction techniques are necessary to improve retention of usable propellants. One idea developed over recent years is to employ zero-boil-off technology (ZBOT) [3, 29–31]. While ZBOT approach was demonstrated to be successful in the case of cryogens with higher boiling points, e.g. LOX, no cryocoolers enabling ZBOT yet exist that could operate at LH₂ temperatures [32]. Another idea to further decrease the heat inflow into the LH₂ tank is to use the concept of broad area cooling (BAC), whereby the tank is surrounded by a network of tubes carrying a coolant fluid [6, 12, 30, 32, 33]. Circulating the fluid through the tubes with the subsequent heat removal by cryocoolers operating at higher temperature may then allow to significantly reduce heat penetration. Use of vapor-cooled shield (VCS) [6, 7, 13, 34] would be particularly efficient, since thermalizing GH₂ with the outer layers of the MLI could increase the storage time up to a factor of 6 (see Secs. III.1.3 and III.1.4 for more details). We note, however, that strong localized heat leaks through MLI penetrations (the main subject of the present paper) provide one of the greatest CFM challenges for long-term cryogenic storage.

III Physics of long-term cryogenic storage

Let us now perform some basic estimates for the sample 15-ton LH₂ tank whose dimensions were introduced in Sec. II. Since the precise parameters of the MLI performance admit significant variation, we will take an overall heat leak per unit area with an ample margin: $q_0 = 0.4 \text{ W/m}^2$, giving a total heat influx of 80W through the MLI (see also [6, 28]). In addition, we will assume that another 40W of heat enters the tank via penetrations in the form of localized heat sources, giving the total incoming heat flow of $Q_0 = 120\text{W}$. We note that MLI penetrations, such as support struts, feed lines, etc., may provide the greatest

Parameter	Value	Meaning
D_{He}	$5 \times 10^{-9} \text{ m}^2/\text{s}$	Diffusivity of helium in LH2
H_0	12 m	Tank height
P	5 - 15 W	Local heat leak power
Q_0	120 W	Total heat leak
R_0	2.5 m	Tank radius
R_{g0}	1.8 m	Ullage bubble radius
R_{H2}	4,124 J/(kg·K)	Gas constant of hydrogen
R_{He}	2,077 J/(kg·K)	Gas constant of helium
S_0	200 m ²	Tank surface area
T_0	240 K	Exterior environment temperature
T_{L0}	20.3 K	Subcooling temperature
T_{s0}	22 K	Saturation temperature of LH2
V_0	240 m ³	Tank volume
V_{g0}	24 m ³	Ullage volume
c_L	10,820 J/(kg·K)	Specific heat of LH2 at $p = \text{const.}$
c_v	13,030 J/(kg·K)	Specific heat of GH2 at $p = \text{const.}$
c_w	10 J/(kg·K)	Specific heat of aluminum
g_0	9.81 m/s ²	Earth's acceleration of gravity
g	$0 - 10^{-6} g_0$	Microgravity acceleration
h	1 cm	Tank wall thickness
p_0	1.6 atm	Operating pressure
q_0	0.4 W/m ²	Heat flux through the MLI
q_L	$4.35 \times 10^5 \text{ J/(kg·K)}$	Latent heat of LH2 vaporization
β_L	0.0192 K ⁻¹	LH2 thermal expansion coefficient
κ_L	0.101 W/(m·K)	Heat conductance of LH2
κ_v	0.019 W/(m·K)	Heat conductance of GH2
κ_w	20 - 200 W/(m·K)	Heat conductance of aluminum
μ_L	$1.16 \times 10^{-5} \text{ Pa·s}$	Viscosity of LH2
ρ_L	68.7 kg/m ³	Density of LH2
ρ_v	2.07 kg/m ³	Density of GH2
ρ_w	2,700 kg/m ³	Density of aluminum
σ_L	$1.65 \times 10^{-3} \text{ N/m}$	Surface tension of LH2

Table 1: Physical parameters used in the estimates.

challenge in the tank's heat management. For example, taking the characteristic parameters of the orbiter support strut from the Space Shuttle external tank, which is a tubular structure of radius $R \simeq 20$ cm, thickness $d \simeq 5$ mm and length $L \simeq 1$ m, with thermal conductivity $\kappa \simeq 7$ W/(m·K) of Inconel 718 alloy at $T \simeq 100$ K [35], we find that the conductive heat leak into the tank can be estimated as $Q_{\text{strut}} \simeq 2\pi\kappa R d T_0 / L = 11$ W. Note that this formula may significantly underestimate Q_{strut} , since it does not take into account the additional heat entering the strut through its own thermal insulation. Similarly, for a titanium strut with $d \simeq 1$ cm and $\kappa \simeq 15$ W/(m·K) [36] we find $Q_{\text{strut}} \simeq 45$ W, and for Al 2219 strut with $d \simeq 1.5$ cm and $\kappa \simeq 70$ W/(m·K) [37] we find a prohibitively high $Q_{\text{strut}} \simeq 320$ W. In view of the preceding considerations, however, the conductive heat leaks must not exceed several Watts per penetration in order for the tank to remain within the acceptable thermal budget. There is, therefore, a significant trade-off between the structural and thermal properties of the materials used, requiring strong materials with low thermal conductivity and a possible need for external penetration cooling [6].

To proceed, we need to specify the operating parameters for LH2 in the tank. We will assume that the tank is initially at pressure $p_0 = 1.6$ atm, corresponding to the saturation temperature $T_{s0} = 22$ K of LH2 (parahydrogen), and that LH2 is subcooled to $T_{L0} = 20.3$ K,

corresponding to saturation temperature at 1 atm. Here and everywhere below the definitions and values of the parameters of hydrogen used are listed in Table 1 (for pressure p_0 at saturation [38]). Initially, a 10% by volume ullage space with volume $V_{g0} = 24$ m³ is present, pressurized by cold GHe. The required mass of GHe to produce the excess pressure of 0.6 atm is equal to $M_{He} = (p_0 - p_{\text{atm}})V_{g0}/R_{He}T_{L0} \simeq 35$ kg. We note that at large ullage volumes (as LH2 is lost due to boil-off or transfer from the tank), large amounts of cold helium gas are required to pressurize the tank. For example, when the ullage occupies 50% of the tank volume, one would need to supply 175 kg of GHe, respectively. In practice, even greater amounts of helium may be required due to dissolution of GHe in LH2 on long storage timescales (see Sec. III.1.5). The liquid is subcooled in order to avoid the presence of vapor bubbles in the bulk LH2, which are a potential hazard for engine restart, etc.

III.1 Basic thermodynamics

We begin by evaluating the heat budget of the tank and related issues.

III.1.1 Time to saturation

First, let us calculate the time needed for LH2 to come from the subcooled condition to the saturation temperature under an assumption of perfect mixing (e.g. by an active mixer inside the tank) and in the absence of any boiling and active cooling. This time is given by equating the total amount of heat that entered the tank to the increase in the LH2 sensible heat:

$$t_{\text{saturation}}^{\text{mixed}} = c_L \rho_L (V_0 - V_{g0}) (T_{s0} - T_{L0}) / Q_0 \simeq 26 \text{ days.}$$

On the other hand, in the absence of mixing, boiling, and any g -forces the heat will only penetrate from the tank wall to the depth equal to the thermodiffusion length $l = \sqrt{\kappa_L t / (c_L \rho_L)}$ of LH2 in time t . Then the same balance leads to

$$t_{\text{saturation}}^{\text{thermodiffusive}} = c_L \rho_L \kappa_L (T_{s0} - T_{L0})^2 / q_0^2 \simeq 16 \text{ days.}$$

Note that, replacing T_{s0} in this equation with 23K, one can see that in order to achieve a superheat of ~ 1 K at the tank wall (at which nucleate boiling normally occurs in LH2 under normal conditions on earth [39–41]), one would need to wait $t \simeq 40$ days. Finally, for a tank in LEO, taking into account convective transport in microgravity with $g = 10^{-6} g_0$, we obtain for the tank wall temperature T_w an estimate $T_w - T_{L0} \simeq 0.22$ K, which is based on the Nusselt number $\text{Nu}_{R_0} = q_0 R_0 / (\kappa_L (T_w - T_{L0})) \simeq 46$ and the Rayleigh number for these parameters $\text{Ra} = g \beta_L (T_w - T_{L0}) c_L \rho_L^2 R_0^3 / (\mu_L \kappa_L) \simeq 2.8 \times 10^7$, and we used the correlation $\text{Nu}_{R_0} = 0.15 \text{Ra}^{1/3}$ [42, Eq. (9.31)].

Thus, the timescale on which the bulk of LH₂ heats to the boiling point under the considered heat loads in the absence of any other sources and sinks of heat is about 1 month. Note that on such a long timescale heat conductance alone is sufficient to carry the heat into the tank interior.

III.1.2 Time to complete evaporation

On the other hand, assuming that the tank is maintained at constant pressure p_0 , we can find the LH₂ storage time by equation the total heat that entered the tank to the heat needed to vaporize all the LH₂:

$$t_{\text{storage}} = \rho_L (V_0 - V_{g0}) (q_L + c_L (T_{s0} - T_{L0})) / Q_0,$$

about 22 months. In particular, about 700 kg or $\sim 5\%$ by volume, of LH₂ will be lost to boil-off in one month. This also means that cold GHe needs to be supplied at a rate of ~ 16 kg/month to maintain LH₂ at subcooled conditions.

While it will take on the order of one month in the absence of any other heat sinks for the bulk of LH₂ to be heated to the saturation temperature, local boiling may begin soon due to the localized heat sources through penetrations. With the power from those sources equal to $Q_0 - q_0 S_0 = 40\text{W}$ and assuming that the boil-off bubbles remain attached to the hot spots on the tank walls, we can estimate the the rate of boil-off of GH₂ as

$$\dot{M}_{GH2,\text{boil-off}} = \frac{Q_0 - q_0 S_0}{q_L + c_L (T_{s0} - T_{L0})} \simeq 8 \text{ kg/day}. \quad (1)$$

This results in an increase of the tank pressure at the rate of $\dot{p} = \dot{M}_{GH2,\text{boil-off}} R_{H2} T_{s0} / V_{g0} \simeq 0.3 \text{ atm/day}$.

III.1.3 Vapor-cooled shield and broad area cooling

The use of VCS can significantly reduce the amount of boil-off by utilizing sensible heat of the boil-off vapor [6, 7, 13, 34]. If the GH₂ is simply vented overboard, the amount of heat removed from the tank by the vapor will be $Q_{\text{boil-off}} \simeq q_L \dot{m}_{GH2}$, where \dot{m}_{GH2} is the mass flow of GH₂ through the vent. If, on the other hand, the vapor is allowed to thermalize with the outer surface of the MLI at temperature $T_0 \simeq 240\text{K}$ before being vented, the amount of heat removed equals $Q_{\text{VCS}} \simeq (q_L + c_v (T_0 - T_{s0})) \dot{m}_{GH2}$ (taking into account that the specific heat of GH₂ does not vary significantly with temperature in the considered interval [38]). The ratio of the two is given by

$$Q_{\text{VCS}} / Q_{\text{boil-off}} \simeq 1 + c_v (T_0 - T_{s0}) / q_L \simeq 7.5. \quad (2)$$

This means that the use of VCS may reduce boil-off rate for a fixed heat load by over a factor of 7 by intercepting the heat entering into the tank. Further increase in the efficiency may be achieved by passing the warm GH₂

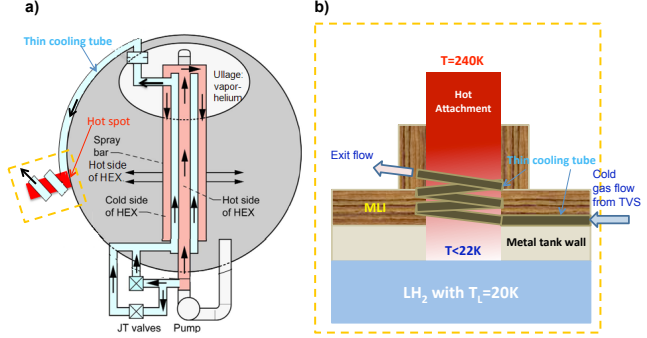


Figure 1: Cooling a penetration by GH₂ from TVS. (a) The tank schematics and (b) the close-up of the cooled penetration. In (a), the TVS schematics is taken from [44].

through para-ortho converters [7].

BAC is another promising concept that takes advantage of actively cooled GHe running through tubes within the MLI to capture the heat entering from the tank environment and allows to significantly reduce the heat flow per unit area through the MLI [32] (see also [33] for a related concept of active co-storage). One of the main difficulties in applying the BAC technology is efficient thermal bonding of the BAC tubing to the tank structures [6, 30]. Recently, both the “tube-to-tank” and the “tube-to-shield” concepts, whereby the BAC tubing is bonded either directly to the tank wall or to an intermediate layer of the MLI, respectively, have been successfully demonstrated [12, 30, 32, 43]. Let us point out that these concepts may also be used as part of a VCS in conjunction with thermodynamic vent system (TVS) [34]. Note, however, that in the absence of boiling inside the tank the VCS/TVS system may not be able to intercept the incoming heat, since the heat entering the tank may raise the LH₂ temperature locally near the tank walls without producing a pressure or bulk LH₂ temperature rise. In this case, the TVS will not operate, and the propellant heating near the tank walls may lead to the potentially dangerous explosive nucleate boiling hazard (see Sec. III.3.2 for more detail). We also note that in order for the tube-to-tank BAC design to work in an LH₂ tank, the cold GHe must be circulated at the temperature of about 20K to avoid boiling of LH₂ at the tank walls. Since no efficient cryocoolers currently exist operating at these temperatures, the tube-to-tank concept is not currently applicable to LH₂ storage.

III.1.4 Heat leak through penetration

One of the most challenging problems in the tank heat management is to control the heat leaks from various MLI penetrations, such as the tank structural supports (struts) and propellant feed lines, see Fig. 1 [6]. As was discussed in Sec. III.1.3, using either VCS or BAC for passive or ac-

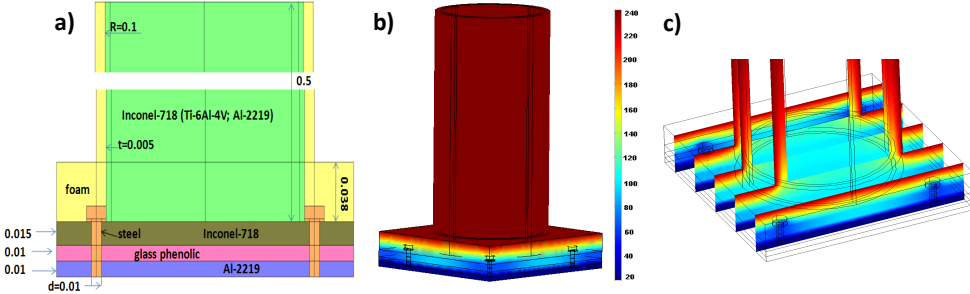


Figure 2: Heat conductance through a simplified fitting assembly, consisting of an Inconel-718 strut bolted to the tank surface through a glass-phenolic isolator. (a) The schematics of the vertical cross-section of the assembly. (b) Temperature distribution on the assembly surface (see color bar for the map to degrees Kelvin). (c) Temperature distribution for several vertical cross-sections. The results are obtained with the help of ANSYS CFX software.

tive cooling of the heat shield, respectively, one could all but eliminate the heat leaks through the MLI into the tank. In this case, the penetrations will provide most of the heat load to the propellant. Note that in contrast to the MLI, where radiative heat transfer dominates, it is not possible to adapt the active tube-to-shield BAC concept operating at intermediate temperatures (see Sec. III.1.3) to intercept most of the heat coming through penetrations because of the dominant role of conductive heat transfer there. A natural idea (an extension of the VCS concept) is, therefore, to sacrifice some of the stored hydrogen to passively cool the penetrations at their points of contact with the tank walls and, in particular, to suppress possible boiling in those areas. The hydrogen is most conveniently supplied by TVS, providing a regulatory feedback between the tank heat load and the amount of LH₂ used for cooling.

Let us assume for simplicity that the tank contains $N_{\text{strut}} = 8$ identical penetration structures (struts). If all the heat enters the tank through penetrations, each strut is assumed to carry heat in the amount of $Q_{\text{strut}} = Q_0/N_{\text{strut}} = 15\text{W}$ conductively into the tank. This number is consistent with the values obtained from the high fidelity computational analysis of heat conduction through a simplified fitting assembly, consisting of a cylindrical Inconel-718 strut 50 cm long, 20 cm in diameter and 5 mm thick covered with a 1 cm thick layer of foam insulation and bolted to the tank surface through a glass-phenolic isolator (Fig. 2). The total heat flux through the assembly into the tank was found to be 32 W. A similar number was found for a strut made of Ti₆Al₄V alloy, and a considerably larger value of 84 W was found for a strut made of Al-2219 alloy. Note that we found that in all cases most of the heat passes into the tank through the attachment bolts.

Under our assumptions about the storage times for the tank, the maximum available LH₂ budget (not including the effect of VCS or BAC) that can be used to cool the

penetrations is

$$J_{\text{strut}} = Q_{\text{strut}}/q_L = 3.3 \times 10^{-5} \text{ kg/s}. \quad (3)$$

This mass flow of cold GH₂ and/or LH₂ can be used, e.g., to locally cool the MLI penetrations in the shape of thick pipes. We consider a helical coil in perfect thermal contact with the strut surface, which is formed by winding a thin hydrogen-carrying tube around the strut (see Fig. 1). Assume that the temperature of GH₂ flowing inside the coil tube that winds around the hot strut changes from $T_v = T_1$ to $T_v = T_2$. By thermodynamic considerations, we must have $Q_{\text{strut}} = c_p(T_2 - T_1)J_{\text{strut}}$. It then follows that the GH₂ supplied at $T_1 = T_{L0} = 20.3\text{K}$ will have the capacity to remove $Q_{\text{strut}} = 15\text{W}$ from the strut, if it is heated to $T_2 \simeq 65\text{K}$.

Let us now estimate the length of the tube which can remove this heat flow. For steady turbulent flow, the heat transfer coefficient h_{tube} can be obtained from the Dittus-Boelter correlation [42]

$$h_{\text{tube}} = \frac{\kappa_v}{2R_{\text{tube}}} \text{Nu}_{\text{tube}}, \\ \text{Nu}_{\text{tube}} \simeq 0.023 \times \text{Re}_{\text{tube}}^{4/5} \text{Pr}_{\text{tube}}^{1/3}, \quad (4)$$

where Nu_{tube} , Re_{tube} and Pr_{tube} are the Nusselt, Reynolds and the Prandtl number associated with the gas flow in the tube, respectively. Note that the formula in Eq. (4) can be equivalently rewritten as

$$h_{\text{tube}} = 0.023c_p \left(\frac{J_{\text{strut}}}{\pi R_{\text{tube}}^2} \right)^{4/5} \left(\frac{\mu_v}{2R_{\text{tube}}} \right)^{1/5} \text{Pr}^{-2/3}, \quad (5)$$

i.e., at fixed J_{strut} the heat transfer coefficient is proportional to $R_{\text{tube}}^{-9/5}$ and, therefore, grows rapidly with decrease of R_{tube} . Considering a tube of radius $R_{\text{tube}} = 2\text{ mm}$, we find that for the mass flow given by Eq. (3) we

have $\text{Re}_{\text{tube}} \simeq 10^4$ and $\text{Pr}_{\text{tube}} \simeq 0.8$, giving the Nusselt number $\text{Nu}_{\text{tube}} \simeq 32$ and the heat transfer coefficient $h_{\text{tube}} \simeq 130 \text{ W}/(\text{m}^2 \cdot \text{K})$. This corresponds to the power $P_{\text{loop}} \simeq 4\pi^2 R_{\text{tube}} R_{\text{strut}} h_{\text{tube}} (T_{s0} - T_{L0}) = 1.8 \text{ W}$ taken away by the first loop of the tube, which is insufficient to take away all the heat. Let us note that by the Darcy-Weisbach equation [45, 46] the pressure drop $\Delta p = p_1$ ensures the flow J_{strut} in a tube of this radius and length $L \simeq 200 \text{ m}$.

The analysis of the heat exchange between the strut maintained at $T = T_0$ at the warm end and in thermal contact with several loops of cold GH2-carrying tubes is rather involved and is presented in [47]. The results depend significantly on many factors, including the dimensions and the material of the penetration. Similarly, the ability of the tube to take away the heat from the penetration depends in a non-trivial way on these factors. One should, therefore, carefully consider the heat conduction problem associated with penetrations in order to assess the feasibility of the proposed cooling strategy. One important factor to keep in mind is that, according to the model predictions, the efficiency of the proposed vapor cooling system decreases with an increase in the effective heat conductance coefficient of the strut. The latter must also include the effect of the additional heat conduction pathways introduced by the highly conducting thermal bonding material and the tubes themselves.

III.1.5 Helium dissolution hazard

We point out that at $T_{L0} = 20.3 \text{ K}$ the solubility limit of GHe in LH2 is $\sim 0.5\%$ by weight [48]. Therefore, all LH2 in the tank is capable to absorb up to 75 kg of GHe, which is about 2 times more than the mass $M_{\text{He}} \simeq 35 \text{ kg}$ of GHe in the ullage at the beginning. Let us estimate the time in which GHe may dissolve in LH2. Taking the diffusion coefficient of the dissolved helium $D_{\text{He}} = 5 \times 10^{-9} \text{ m}^2/\text{s}$ (assumed to be of the same order as the available value for neon [49], see also [50]), assuming that the ullage has the shape of a spherical bubble of radius $R_{g0} = 1.8 \text{ m}$ and estimating the diffusive flux at the ullage boundary to be $D_{\text{He}} \rho_{\text{He},\text{sat}} / l_{\text{He}}$, where $\rho_{\text{He},\text{sat}} = 0.005 \rho_L$ is the helium saturation density and $l_{\text{He}} = \sqrt{D_{\text{He}} t}$ is the helium diffusion length, respectively, in LH2, we obtain that in the absence of active mixing the dissolved mass of GHe in time t is

$$\begin{aligned} M_{\text{He,dissolved}} &\simeq 4\pi R_{g0}^2 l_{\text{He}} \rho_{\text{He},\text{sat}}, \\ M_{\text{He,dissolved}} &\simeq 1.6 \text{ kg}, \quad t = 1 \text{ month}. \end{aligned} \quad (6)$$

Let us note that in the presence of active mixing the rate of GHe dissolution may be significantly higher. For example, if LH2 is circulated with an average axial velocity $u_{\text{bulk}} = 1 \text{ mm/s}$ across the tank, then the Peclet number $\text{Pe} = 2R_{g0} u_{\text{bulk}} / D_{\text{He}} \simeq 7 \times 10^5$ for the ullage

bubble. Therefore, the dimensionless Sherwood number $\text{Sh} = 0.65 \text{Pe}^{1/2} \simeq 550$ (see [51, Eq. (3.52)], assuming spherical ullage in a background flow with velocity u_{bulk}), and the dissolution rate becomes $\dot{M}_{\text{He}} = 2\pi R_{g0} D_{\text{He}} \rho_{\text{He},\text{sat}} \text{Sh} \simeq 30 \text{ kg/month}$. Thus, the entire mass of GHe may dissolve in LH2 in only one month, leading to the collapse of the ullage pressure. The dissolution rate may further increase due to ullage bubble motion. Therefore, on the long-term storage timescales one needs to evaluate the potential ullage collapse hazard due to GHe dissolution in LH2. One also needs to take into consideration the possible effect of dissolved non-condensable helium gas on the boiling characteristics [20, 52, 53].

III.2 Pressure control

When the sufficient level of superheat is reached at the tank walls and/or enough heat enters through penetrations, nucleate boiling will start. As vapor is created due to boil-off, the tank pressure rises, requiring venting in the absence of heat removal. As was shown in Sec. III.1, with the considered heat leak the excess pressure $p_0 - p_{\text{atm}}$ will increase by a factor of two in just 2 days in the absence of venting.

In microgravity, venting becomes an issue, since the location of the ullage space in the tank is not known and, therefore, it is not possible to guarantee that vapor, not liquid, is vented in the process. Note that venting LH2 caused the vehicle to tumble out of control during the AC-4 test flight in 1964 [8, 9]. To circumvent this problem, TVS technology is proposed, in which the two-phase mixture of liquid and vapor may be expanded in a Joule-Thompson device and then passed through a heat exchanger to take away heat from the warmer fluid in the tank, see Fig. 3 for schematics [6, 10, 30, 44]. We note that ideally the work of TVS would result in the LH2 loss rate equal to that of a tank with the same heat budget venting the vapor directly overboard. In practice, increased losses are inevitable due to finite TVS efficiency.

The basic physical principle of TVS operation is to control tank pressure by keeping the bulk LH2 at subcooled conditions. Therefore, successful operation of TVS relies crucially on its ability to efficiently move heat from the regions of nucleate boiling to the TVS heat exchanger inside the tank by utilizing fluid mixers, such as an axial jet or spray bars. We note that, on one hand, LH2 circulation must be sufficiently strong in order for the heat through penetrations to be removed from vapor bubbles. On the other hand, if the circulation is too strong, then the ullage bubble may be distorted or fragmented, resulting in its possible capture by the TVS intake.

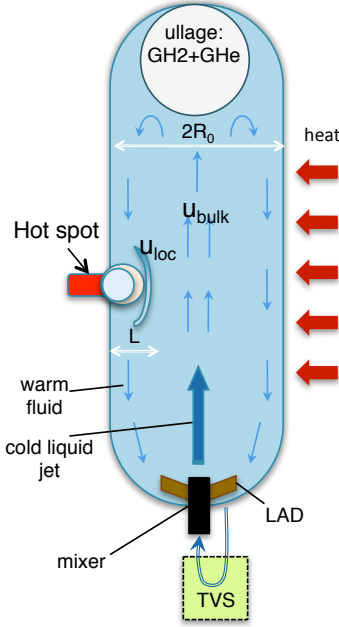


Figure 3: A Tank/TVS configuration with an axial jet mixer. Blue arrows indicate LH2 circulation; red arrows indicate heat influx through the MLI; on the left, a vapor bubble is attached to a hot spot (red) at the point of a localized heat leak through a penetration.

III.2.1 TVS hazard induced by ullage motion

In microgravity the ullage containing the saturated vapor and helium can drift to the TVS intake and become captured by it. This dangerous effect is unexplored. It may cause the TVS to cease normal operation. Bubbles containing helium may come out of the TVS, decreasing the helium mass in the main ullage. These effects may cause generation of many new bubbles with GHe and the formation of the multi-phase liquid-gas foam instead of the regular ullage. It maybe then be impossible to annihilate this foam by pre-start pressurization, since the collapsing bubbles will contain non-condensable helium gas.

To estimate the critical LH2 circulation velocity u_{bulk} , above which the ullage motion hazard becomes significant, we compute the flow Weber number $We = 2\rho_L u_{bulk}^2 R_{g0}/\sigma_L$. The flow will begin to affect the shape of the ullage bubble when the Weber number $We \gtrsim 1$; for example, for $u_{bulk} = 5 \text{ mm/s}$ we will have $We \simeq 4$, indicating the onset of ullage motion [19].

III.2.2 Boiling near hot spots

Let us now estimate the rate of heat removal from a bubble growing near a hot spot at the tank wall. A detailed treatment of this question is difficult without specifics of the LH2 flow pattern, which depend on the tank design

(see [31, 54] for recent numerical studies). Therefore, for simplicity we will assume that LH2 flow is generated by the axial jet which creates a counterflow pattern (see Fig. 3), in which LH2 moves with average velocity u_{bulk} in the region $r < R_0 - L$, where r is the distance to the tank axis, and with average velocity $u_{counter}$ in the opposite direction in a layer of thickness L next to the tank wall. Since at the wall the flow velocity is zero, in a laminar flow the magnitude of the LH2 velocity next to a bubble of radius R may be estimated as $u_{loc} \simeq 4Ru_{counter}/L$, where we used linear interpolation from $u = 0$ at $r = R_0$ to $u = 2u_{counter}$ at $r = R_0 - L$ for the axial liquid velocity u . From mass conservation we find that

$$u_{loc} \simeq 4Ru_{bulk}(R_0 - L)^2/(2R_0L^2 - L^3). \quad (7)$$

Taking $L \simeq 1 \text{ m}$ and the value of $u_{bulk} = 5 \text{ mm/s}$ obtained in the preceding paragraph, one can see that a localized heat source with power $P = 5 \text{ W}$ may produce a steady bubble of radius $R \simeq 13 \text{ cm}$. This follows from the balance of heat, taking into consideration that the Nusselt number $\text{Nu}_R = P/(2\pi R\kappa_L(T_{s0} - T_{L0})) \simeq 35$ for the bubble can be correlated as $\text{Nu}_R = 0.65\text{Pe}_R^{1/2}$ with the Peclet number $\text{Pe}_R = 2u_{loc}Rc_L\rho_L/\kappa_L \simeq 3000$ in this case (see [51, Eq. (3.52)]), assuming small contact angle and, hence, an almost spherical bubble, and ignoring the presence of the wall for the flow for simplicity). Similarly, a bulk velocity $u_{bulk} = 1 \text{ mm/s}$ would result in a steady bubble of radius $R = 20 \text{ cm}$. We note that even with this smaller value of the circulation speed u_{bulk} one would need to supply LH2 through the axial jet at the rate $G_{LH2} = \pi(R_0 - L)^2\rho_L u_{bulk} \simeq 0.5 \text{ kg/s}$, which, for an axial jet with an orifice of 10 cm diameter would require the fluid velocity of about 1 m/s. The corresponding circulation time for the whole tank would be 8 hours in this case. At the same time, for a given leak power the system will not be able to control the growth of bubbles attached to hot spots whose radii are smaller.

III.3 Dynamics of bubble growth and collapse

We now discuss the dynamics of vapor bubbles inside LH2 in more detail.

III.3.1 Onset of bubble nucleations at hot spots

Let us begin by estimating the time needed for a single bubble to appear near a localized heat leak with power $P = 5 \text{ W}$. We assume that the heat enters the tank through a penetration connected to the exterior side of an aluminum LH2 tank. We note that in contrast to the Apollo design, in which thermal insulation was on the interior tank surface [16], the MLI has to be installed on the tank's exterior surface, since it needs to operate in vacuum. Hence, in the absence of any special inner surface coating, the stored LH2 will be in contact with a highly

conductive metal surface. At $T_{L0} = 20.3\text{K}$, heat conductance κ_w of the tank wall lies in the range of $20 - 200 \text{ W}/(\text{m}\cdot\text{K})$, depending on the composition of the aluminum alloy used [13, 55]. Also note that bubble inception superheat will be higher than the one needed to maintain nucleate boiling and will vary depending on the tank wall finish [20, 56–58].

Suppose first that LH2 is at the subcooled temperature T_{L0} when the heat leak is applied. Because of the much higher heat conductance of aluminum, this heat will first spread into the tank wall. If $l_w = \sqrt{\kappa_w t}/(c_w \rho_w)$ is the thermodiffusion length of aluminum, then one can roughly estimate the temperature increase in the tank wall by equating the amount of heat Pt entering aluminum in time t to the heat content $\pi l_w^2 h c_w \rho_w (T - T_{L0})$ of a cylindrical section of the tank wall with radius l_w and thickness h . The timescale of temperature spreading may also be estimated by equating l_w to r_0 :

$$t_w = c_w \rho_w r_0^2 / \kappa_w \simeq 0.3 \text{ s} \div 3 \text{ s}, \quad (8)$$

where $r_0 \simeq 5 \text{ cm}$ is the radius of the penetration. A more precise analysis [47] gives an extra logarithmic factor in the expression for the maximum temperature in the hot spot:

$$T \simeq T_{L0} + P/(4\pi h \kappa_w) \ln(6.1t/t_w). \quad (9)$$

Taking $h = 1 \text{ cm}$, we find that for $t = 3t_w$ the value of T varies in the range $21\text{K} - 26\text{K}$, depending on the heat conductance κ_w . Therefore, three distinct scenarios are possible, depending on the values of κ_w and P in the absence of boiling.

The first scenario is realized, if the heat leak power P is sufficiently high and the heat conductance κ_w is sufficiently low. For the considered value of P and $\kappa_w = 20 \text{ W}/(\text{m}\cdot\text{K})$, which is at the low end of the range of κ_w , by Eq. (9) we get $T \simeq 24\text{K}$ already at $t = t_w = 3 \text{ s}$. This corresponds to superheat of 2K , already above the nominal 1K superheat for the nucleate boiling onset in LH2 [39–41]. In this situation, nucleate boiling will start immediately, with all the heat going into a single vapor bubble.

The second scenario is realized when the heat conductance κ_w is sufficiently high. Then in the presence of losses through convection the heat from the leak spreads to distances up to [47]

$$l_s = (\kappa_w h R_0 / (\kappa_L \text{Nu}_{R_0}))^{1/2}, \quad (10)$$

where Nu_{R_0} is the Nusselt number associated with convection. The maximum temperature in the hot spot can be estimated as [47]

$$\max T \simeq T_{L0} + P / (2\pi \kappa_w h) \ln(1.85l_s/r_0). \quad (11)$$

For example, with $\kappa_w = 200\text{W}/(\text{m}\cdot\text{K})$, corresponding to the high end of the range of κ_w , and $\text{Nu}_{R_0} \simeq 46$ estimated in Sec. III.1 for free convection in microgravity, we obtain $l_s \simeq 1 \text{ m}$. About the same Nusselt number is also obtained for forced convection with average velocity $u_{bulk} = 1 \text{ mm/s}$ considered in Sec. III.1, using the correlation [42, Eq. (7.23)]

$$\text{Nu}_{R_0} = 0.332 \times \left(\frac{\rho_L u_{bulk} R_0}{\mu_L} \right)^{1/2} \left(\frac{c_L \mu_L}{\kappa_L} \right)^{1/3} \simeq 44.$$

Then, according to Eq. (11), we get $\max T \simeq 21.8\text{K}$, so the temperature in a hot spot remains below the saturation temperature, and the heat is removed convectively from the leak, as desired. Note that in zero gravity and absence of any boiling or mixing the value of l_s in Eq. (11) should be replaced with R_0 , and the value of T_{L0} should be replaced with the spatially averaged tank temperature T_{w0} . The latter will be increasing on the timescale $t_{\text{sat}}^{\text{thermodiffusion}}$ (see Sec. III.1), eventually leading to nucleate boiling. On the other hand, an addition of an active mixer next to a hot spot will further reduce the value of l_s and, therefore, further suppress boiling. This may be a better strategy for mitigating the effect of heat leaks through MLI penetrations (compare with the strategies discussed in Sec. III.1.4).

The third scenario is realized when the wall heat conductance is low, and the heat leak power is also sufficiently low, provided that convective heat transfer is negligible. The latter takes place, e.g., in zero gravity and in the absence of active mixing. We consider this scenario in more detail in Sec. III.3.2.

III.3.2 Explosive nucleate boiling hazard

If the power P is not sufficient to initiate nucleate boiling quickly in time t_w , then, according to Eq. (9) it may take an exponentially long time for the wall temperature to reach the required superheat, resulting in a long delay in the onset of nucleate boiling. Consider, for example, the case of $\kappa_w = 20 \text{ W}/(\text{m}\cdot\text{K})$ and $P = 1\text{W}$. Then, by Eq. (9) a temperature $T \simeq 24\text{K}$ corresponding to a 2K superheat will only be reached at $t = 1.4 \text{ hours}$. In this time the heat will spread to $l_w \simeq 2 \text{ m}$ along the tank wall and $l_L \simeq \sqrt{\kappa_L t / (c_L \rho_L)} \simeq 2.6 \text{ cm}$ into LH2. When nucleation occurs, the heat stored in this superheated layer of LH2 will be used to convert a mass m_{H2} into vapor, with $m_{H2} \simeq \pi l_w^2 l_L c_L \rho_L (T - T_{s0}) / q_L = 1 \text{ kg}$ for the considered parameters. The resulting vapor volume $V \simeq 0.5 \text{ m}^3$ will then be violently released into the tank in a short time. This is an example of the phenomenon of explosive nucleate boiling [57–59] that was ubiquitously observed in the microgravity boiling experiments on board the Space Shuttle Columbia [60]. We note that the accompanying pressure spike may present a potential hazard for

the operation of the storage tank. Moreover, many vapor bubbles may be injected into LH₂ as a consequence of explosive boiling, contributing to the formation of liquid-vapor foam.

Let us note that in the absence of mixing the size of the hot spot is limited by the length scale $L = h\kappa_w/\kappa_L$ [47]. Assuming that $\kappa_w \simeq 20 \text{ W/(m}\cdot\text{K)}$, as before, we find that $L \simeq 2 \text{ m}$. Correspondingly, the maximum temperature in the hot spot is limited by the expression given by Eq. (11) with l_s replaced by L [47]. However, in this case the steady state superheat will extend into the liquid also to the length L , creating a much larger mass of superheated LH₂, whose explosive boiling may be catastrophic.

III.3.3 Bubble growth over a hot spot

Once a vapor bubble is nucleated, it will grow by drawing the heat from surrounding superheated liquid which, in turn, receives heat from hot spots on the tank wall. We note that for small heat fluxes considered here the dominant heat transfer mechanism will be transient heat conduction (for a recent discussion of different growth mechanisms, see [61]).

Assuming that all the power from a localized heat leak is used to convert liquid into vapor in a single bubble, the bubble radius as a function of temperature, or, equivalently, the growth time for a bubble of a given radius, are

$$R = (3Pt/(4\pi\rho_v q_L))^{1/3}, \\ t_{\text{growth}} = 4\pi\rho_v q_L R^3/(3P). \quad (12)$$

With $P = 5\text{W}$, we then find that $t_{\text{growth}} = 1.7 \text{ hour}$ for $R \simeq 20 \text{ cm}$ and $t_{\text{growth}} = 6 \text{ sec}$ for $R \simeq 2 \text{ cm}$. Note the difference in the dependence of the bubble radius R on t with the classical $t^{1/2}$ dependence obtained in [62, 63] (see also [64, 65]). This is due to the fact that the bubbles under consideration grow near a hot spot on a thin strongly conductive tank surface. Therefore, the heat flux into the bubble is mediated by the high heat conductance through the tank wall (for a recent discussion of the importance of heat conductance in the heater during nucleate boiling, see [66–68]). We note that if our assumption that a significant portion of the heat flow from the localized heat leak flows into the bubble were violated, then the bubble would only act as a small perturbation for the temperature distribution in the tank wall. Therefore, to the leading order the maximum temperature there would still obey Eq. (11). However, this is inconsistent with the assumption of no boiling at the tank surface, if the maximum superheat governed by Eq. (11) exceeds 1K.

Note that far from the hot spots Eq. (12) remains valid, if one sets $P = q_0 A$, where A is the wall area per bubble. The latter is valid in the case of high heat conductance of the tank wall, when on average each bubbles will be able to intercept all the heat entering through the area A of the

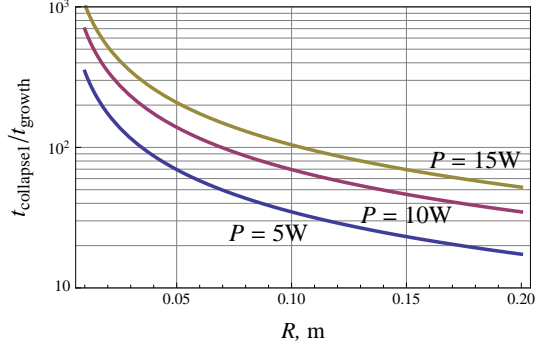


Figure 4: The ratio of the bubble collapse time to the bubble growth time as a function of the bubble radius at departure.

tank wall. For example, for $A = L^2$, with $L = 10 \text{ cm}$, we find that the bubbles will reach $R = 2 \text{ cm}$ in $t \simeq 2 \text{ hours}$. When neighboring bubbles at the tank wall grow large enough to come in contact with each other, more complicated dynamics involving coalescence and detachment from the tank wall will occur. The latter phenomenon was recently demonstrated to be important in the experiments conducted in the low gravity environment of the NASA's KC-135 aircraft [69–71].

III.3.4 Bubble collapse and accumulation in the subcooled liquid

As a result of several possible bubble departure mechanisms, vapor bubbles may detach from the tank wall and enter into the bulk liquid. Several scenarios are possible here, depending on the size of the departing bubbles, the level of microgravity, and the liquid flow rate. Larger bubbles may rise toward the area of zero gravity (the tank mid-plane for a tank in a circular LEO) under the action of buoyancy forces. The rise time may be estimated by balancing the buoyancy force $\frac{4}{3}\pi R^3 \rho_L g$ with viscous drag $4\pi\mu_L Ru$, where $u \simeq R_0/t_{\text{rise}}$ is the bubble velocity relative to the liquid (recall that R_0 is the tank radius) [51], to obtain

$$t_{\text{rise}} = 3\mu_L R_0/(\rho_L g R^2) \simeq 5 \text{ min}, \quad R = 2 \text{ cm}, \quad (13)$$

which is decreasing with the increase of bubble radius R . These bubbles may then be swept towards the ullage bubble by the flow generated by the mixer and coalesce with it (see Fig. 3). The timescale of this process is given by

$$t_{\text{flow}} = H_0/u_{\text{bulk}} \simeq 3 \text{ hours}, \quad u_{\text{bulk}} = 1 \text{ mm/s}. \quad (14)$$

Note that by the estimates of Sec. III.3.3 it takes much longer for a bubble to reach the ullage than to grow to the considered size. Hence bubbles may accumulate in the liquid and be carried by the flow and deposited in its

stagnation areas.

Let us estimate the bubble lifetime, assuming that upon departure it enters the region of the subcooled LH₂. Assuming first that the heat escapes the bubble via steady conduction and equating the conductive heat flow $4\pi R^2 \kappa_L (T_{s0} - T_{L0})/R$ to the heat release rate $4\pi R^2 (dR/dt) \rho_v q_L$ due to condensation, and then solving the obtained differential equation, we obtain the time for the bubble of radius R to collapse into the subcooled liquid:

$$t_{\text{collapse1}} = q_L \rho_v R^2 / (2\kappa_L (T_{s0} - T_{L0})). \quad (15)$$

Note that this equation is asymptotically exact in the limit of vanishing subcooling, but underestimates $t_{\text{collapse1}}$ for larger subcoolings due to the condensation blocking effect [72]. Indeed, assuming that the condensation rate is dominated by the conduction through the thermal boundary layer of width $l = \sqrt{\kappa_L t / (c_L \rho_L)}$, one should replace the factor $1/R$ by $1/l$ in the expression for the heat flux to obtain [47]

$$t_{\text{collapse2}} = \pi \rho_v^2 q_L^2 R^2 / (4 c_L \rho_L \kappa_L (T_{s0} - T_{L0})^2). \quad (16)$$

The blocking mechanism is not important when $t_{\text{collapse1}} \lesssim t_{\text{collapse2}}$, which is the case in the examples that follow.

From Eq. (15), one can see that a bubble of radius $R = 20$ cm will have a lifetime $t_{\text{collapse1}} \simeq 30$ hours ($t_{\text{growth}} \simeq 1.7$ hour). For smaller bubbles with, say, $R = 2$ cm, we have $t_{\text{collapse1}} \simeq 20$ mins ($t_{\text{growth}} \simeq 6$ sec). Note that these estimates agree very well with the results of direct numerical simulations of the full system of hydrodynamic equations describing the bubble collapse [47]. Once again, in the considered case the bubbles are produced faster than they are collapsing in the subcooled liquid, i.e. $t_{\text{growth}} \ll t_{\text{collapse}}$ (Fig. 4). Note, however, that as the bubbles collapse, they release heat into the liquid, so that the subsequent bubbles are exposed to a smaller degree of subcooling. Therefore, as more bubbles arrive, their lifetime may steadily increase and the liquid around them reach saturation, resulting in the formation of stable bubble colonies. These colonies then contribute to the formation of the multiphase liquid-vapor foam.

III.3.5 Formation of a multi-phase liquid-vapor foam

The above estimates assumed that the bubble receiving power P from the heat leak remains attached to the hot spot at all times. In microgravity, bubbles will have a much reduced tendency to detach from the wall and rise towards the ullage [20, 69–71]. Using the correlation of Fritz [17, 73], we find that the bubble radius at departure in microgravity can be estimated at $R_d \simeq 30$ cm, assuming, e.g., a contact angle $\gamma \simeq 20^\circ$ (small contact angles with metal surfaces are characteristic of LH₂, a strongly

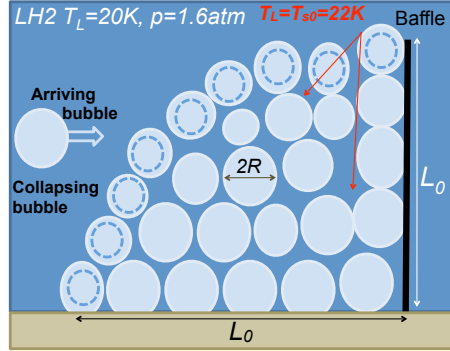


Figure 5: Formation of a foam-like bubble colony in the stagnation area of the stirring flow near a baffle.

wetting liquid [64, 73]). Note that the Weber number for the bubble $We_R = 2\rho_L u_{loc}^2 R / \sigma_L \simeq 0.005$ is small in this case, and so the bubble may not be blown off easily from the hot spot by the flow. If the bubble departure radius R_d exceeds the steady bubble radius obtained above, the bubble will stop growing and assume its steady-state radius, and the heat will be transferred from the hot spot through the bubble to the liquid, as desired.

The departure radius is proportional to the contact angle [17, 73] and becomes smaller than the steady-state bubble radius estimated in the preceding paragraph for contact angles $\gamma \lesssim 10^\circ$. Thus, for these smaller contact angles bubbles will be leaving the area of the hot spot and entering into the bulk liquid. Other mechanisms of bubble departure, such as bubble coalescence, *g*-jitter, and the effect of the liquid flow [17, 65, 74], which are found to be important under reduced gravity conditions [69–71], may further reduce the bubble departure radius. As a result, bubbles may be injected into the liquid and start to move with the flow, reaching, in particular, the flow stagnation areas.

Continuously arriving and collapsing bubbles will raise the temperature in the stagnation areas above the subcooling temperature $T_{L0} = 20.3$ K (Fig. 5). Balancing the latent heat $\frac{4}{3}\pi R^3 \rho_v q_L$ released by vapor condensation of a bubble of radius R with the increase in the sensible heat $\frac{4}{3}\pi R_{hL}^3 \rho_L c_L (T_{s0} - T_{L0})$ of a liquid sphere of radius R_{hL} , we find that

$$R_{hL}/R = (\rho_v q_L / (\rho_L c_L (T_{s0} - T_{L0})))^{1/3} \simeq 1. \quad (17)$$

Thus, the volume of the heated liquid is approximately equal to the volume of the collapsed bubble. As a result, the liquid in the stagnation areas will heat up to the saturation temperature, and the arriving bubbles will stop collapsing and will accumulate in those regions (see Fig. 5). Thus, when bubbles arrive there, a complex multi-phase liquid-vapor foam-like mixture may form with tempera-

ture at saturation. The bubble colonies forming in this way may further thermally insulate the tank walls from the subcooled liquid and result in the formation of more bubbles through nucleate boiling, making TVS cooling ineffective.

For bubble colonies to form, it is necessary that the bubbles generated near the hot spots and then carried by the flow do not have enough time to collapse on the way to the stagnation areas. We can estimate the arrival time of a bubble to the colony by $t_{\text{arrive}} \simeq L/u_{\text{bulk}}$, where L is the distance from a hot spot to the stagnation area and u_{bulk} is the characteristic flow velocity. Using $u_{\text{bulk}} = 5 \text{ mm/s}$ as in Sec. III.2.2 and $L = 0.5 \text{ m}$, we obtain $t_{\text{arrive}} = 100 \text{ sec}$. At the same time, a bubble of radius $R = 2 \text{ cm}$ needs $t = 30 \text{ mins}$ to collapse (see Sec. III.3.4 below), and this time rapidly increases with the bubble size. So bubbles that are not too small will be able to reach the colony. At the same time, if one considers an isolated bubble colony of characteristic size L that is shrinking due to conductive heat transfer, we can estimate the amount of shrinking by balancing the conductive heat flow $L^2 \kappa_L (T_{s0} - T_{L0})/l$, where $l = \sqrt{\kappa_L t / (c_L \rho_L)}$ is the thermodiffusive length in the liquid, with the amount of heat $3L^2(dL/dt)q_L \rho_v f$, where f is the bubble volume fraction, released through condensation in unit time. Integrating the obtained equation, one obtains that the amount of shrinkage in time t is

$$\Delta L \simeq \sqrt{\kappa_L c_L \rho_L t} (T_{s0} - T_{L0}) / (f q_L \rho_v). \quad (18)$$

From this equation one can see that in the absence of any incoming bubbles a foam region of size $L = 0.5 \text{ m}$ and volume fraction, say, $f = 0.2$ would collapse in time $t \simeq 10 \text{ hrs}$. Note that the average power $P = f q_L \rho_v L^3/t \simeq 0.6 \text{ W}$ released in this process is 25 times less than the heat injected into the hot spot for $Q_{\text{strut}} = 15 \text{ W}$. Therefore, when the bubbles arrive from the hot spot, the colony will grow. Note that to include the effect of forced convection in the liquid, we need to replace the thermodiffusive length above with $l = L/\text{Nu}_{R_0}$, where $\text{Nu}_{R_0} \simeq 44$ is the Nusselt number (see Sec. III.3.1 below). Then balancing the heat flow Q_{strut} through the penetration with the heat removed from the colony, we find that the critical colony size, beyond which it will stop growing is

$$L \simeq Q_{\text{strut}} / (\kappa_L \text{Nu}_{R_0} (T_{s0} - T_{L0})), \quad (19)$$

which for $Q_{\text{strut}} = 15 \text{ W}$ gives $L \simeq 2 \text{ m}$.

III.3.6 Bubble collapse by pre-start pressurization

The presence of vapor bubbles in LH2 is highly undesirable for the engine restart, since those bubbles may enter into engine feed lines and result in cavitation of the turbopumps [1]. A way to reduce or eliminate the vapor bubbles prior to engine restart is to pressurize the tank with

GHe and, at the same time, apply a small settling thrust from ullage engines. Pressurization changes the LH2 saturation temperature relative to the bulk liquid temperature, making vapor bubbles to condense.

Several issues arise in the course of pre-start pressurization which may result in an incomplete vapor bubble collapse, making the procedure inefficient. First, bubble condensation releases heat into the bulk liquid, increasing its temperature and potentially bringing it to the new saturation temperature and stopping further condensation. This is particularly relevant to the vapor bubble colonies. Consider, for example, the case in which the tank originally at pressure $p_0 = 1.6 \text{ atm}$ is pressurized to a new pressure $p = 2 \text{ atm}$. The corresponding new saturation temperature is $T_s = 23 \text{ K}$. Now, suppose a bubble colony, which remains at the old saturation temperature $T_{s0} = 22 \text{ K}$ has vapor volume fraction f . Then the total amount of heat this foam-like multiphase fluid can absorb is

$$Q = (1 - f) c_L \rho_L V (T_s - T_{s0}), \quad (20)$$

where V is the colony volume. This amount of heat, in turn, can condense only the volume $V_{\text{cond}} = Q/(q_L \rho_v)$ of the vapor. Comparing the value of V_{cond} with the total vapor volume fV , we can see that by purely thermodynamic considerations all the bubbles will not be able to condense, if

$$f \geq (1 + \rho_v q_L / (c_L \rho_L (T_s - T_{s0})))^{-1} \simeq 0.45. \quad (21)$$

In other words, it will not be thermodynamically possible to condense all the vapor, if the volume fraction of vapor exceeds a critical value given by Eq. (21).

On the other hand, even if the volume fraction f of vapor is below the critical value, vapor condensation may not occur during the time interval of pressurization due to the general slowness of the condensation process and, in particular, due to the condensation blocking phenomenon for larger bubbles. One can once again use Eqs. (15) and (16) in these two regimes to estimate the collapse time for bubbles of different size, provided that $T_{s0} - T_{L0}$ is replaced with $T_s - T_{s0}$. Using these formulas, we now find that $t_{\text{collapse1}} = 30 \text{ mins}$ for $R = 2 \text{ cm}$, or $t_{\text{collapse1}} = 50 \text{ hours}$ for $R = 20 \text{ cm}$. It is clear that larger bubbles may not be eliminated by pressurization in a reasonable time. However, by a settling acceleration $g \sim 10^{-4} g_0$ it is possible to move larger bubbles toward the ullage. Using Eq. (13) with R_0 replaced by H_0 , we find that bubbles of radii $R \geq 5 \text{ mm}$ will be able to move towards the ullage in time $t_{\text{rise}} = 5 \text{ mins}$. At the same time, for smaller bubbles the collapse time is bounded above by $t_{\text{collapse1}} \simeq 2 \text{ mins}$, assuming the best case scenario given by Eq. (15). This indicates that there are rather tight constraints for achieving the desired result from pre-start pressurization. Also note that during pre-start pressurization bubbles will be

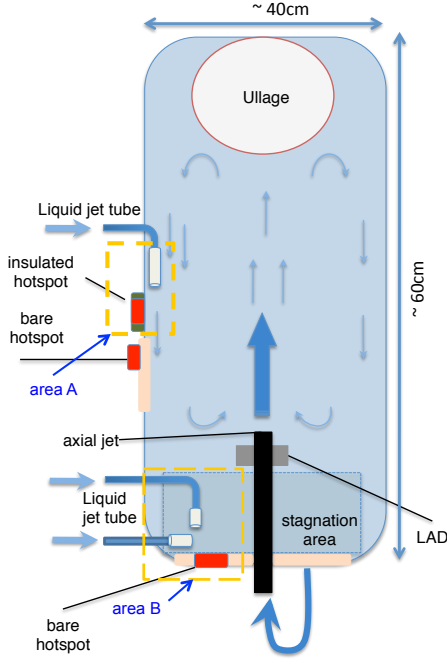


Figure 6: Conceptual design of the test tank.

continuously generated at the hot spots. Provided their departure radius is below 5 mm, these bubbles will not be eliminated at the moment of engine start. In addition, larger bubbles forming inside the engine's start box, if any, will be trapped by the capillary screens of the liquid acquisition device (LAD) and will not be able to rise to the ullage. Finally, helium-filled bubbles forming as a result of a possible ullage capture by the TVS intake cannot be eliminated by pre-start pressurization.

IV A concept for a medium-scale cryogenic tank microgravity experiment

Both theoretical and experimental understanding of the fundamental processes governing long-term cryogenic propellant storage in microgravity are needed to develop tank designs and rapid chilldown technology for LH₂, as well as LOX and other cryogenic liquids. These processes may be studied with the help of an intermediate scale liquid nitrogen (LN₂) or LOX tank. For safety reasons, we chose to concentrate on an LN₂-based design. Here LN₂ plays the role of a LOX simulant, because of the similarity of the parameters of the two liquids. We note that the same parameters may be used for a LOX-based tank, should the safety considerations not be critical.

We propose a conceptual design of an experimental apparatus to study nucleate boiling phenomena for cryogens subject to localized heating on board the International Space Station (ISS). The apparatus consists of a test tank, in which the experiments will take place, a high-pressure

LN₂ delivery tank (e.g., based on the Shuttle PRSD Tank), a high pressure GHe supply tank, a vented enclosure and the necessary support and electronics. The test tank is a cylindrical tank capable of holding $M_{LN_2} \simeq 50$ kg of LN₂, containing an internal LAD, an axial jet mixer, TVS, cryocooler, cryotrackers, GHe diffuser, an external MLI blanket reducing the surface heat flux into LN₂ to $q_h = 0.2$ W/m² on orbit, and a TVS-fed VCS line wrap. During launch, the test tank is empty and the delivery tank is filled with LN₂. Once on orbit, LN₂ is transferred to the test tank, allowing a study of rapid on-orbit tank chill-down. Upon filling, the overpressure in the test tank is maintained by an addition of GHe from the GH₂ supply tank. The apparatus is expected to operate in orbit for a period of one year.

The test tank is equipped with a pressure sensor, a system of thermo- and wet/dry sensors, boroscopes near the insulated and bare (on the tank wall) heaters, and miniature liquid jet feed tubes. The basic requirements for the sensors are the operating frequency ≥ 10 Hz and the temperature range 65K \div 300K. The thermosensor set may be substituted by Distributed Fiber Bragg Grating Temperature Sensor Cables, and the wet/dry sensors by Optical Fiber Boroscopes for visible light. The maximum power from each localized heater that simulates MLI penetrations is $P_{loc} \simeq 0.5$ W. Figure 6a shows a possible overall tank design. One area of the tank (area A) corresponds to a hot spot in contact with circulating liquid. Another area (area B) corresponds to a hot spot in contact with stagnant liquid.

This setup should allow to study the on-orbit chill-down process, the growth and detachment of vapor bubbles near the hot spots, the collapse of the detached bubbles in the sub-cooled liquid, the accumulation of bubbles in the stagnation areas and formation of foam-like multiphase fluid, and bubble colony removal by an additional pressurization.

V Conclusions

Recent developments in cryogenic technology will soon enable the design of long-term cryogenic storage tanks that have extremely low heat leaks per unit area of the tank surface. In this situation, localized heat leaks through the tank structural supports, feed lines and other MLI penetrations start to play the dominant role in the tank's heat balance.

Our analysis demonstrates that in the case of LH₂ these localized heat leaks are a serious concern. This is due to the fact that, according to our estimates, the heat flow through the MLI penetrations will be sufficiently high, and, therefore, intense nucleate boiling at the hot spots on the tank surface next to those penetrations is *inevitable*. Moreover, the characteristic growth time for the bubbles

will be considerably smaller than the time of bubble collapse due to condensation in the subcooled liquid. Therefore, vapor bubbles may be generated faster than they are removed. Note that while we mainly based our conclusions on the analysis of metallic tanks, this problem is even more acute for composite tanks due to their low lateral thermal conductivity.

The vapor bubbles that are generated by local nucleate boiling may drift with the liquid flow due to mixing or microgravity and accumulate in the stagnation areas of the flow. Bubble collapse due to condensation heats the surrounding liquid and may lead to growth of the volume occupied by the vapor due to the formation of a multi-phase warm liquid-vapor foam. This foam may not be easily removed by a rapid pressurization. A rapid rise of pressure will cause the relative volume of the vapor in the foam to decrease, but at the same time the surrounding liquid will heat up to the new saturation temperature at that pressure. Let us also point out that the use of GHe to maintain constant overpressure in the tank is associated with He dissolution hazard, whereby the pressurant He gas may dissolve in LH₂ on long storage time scales. The latter would require greater amounts of GHe for maintaining overpressure and may also affect the boiling characteristics of LH₂.

We emphasize that the optimal design of the LH₂ and LOX long-term on-orbit and deep space storage tanks is impossible without joint theoretical and experimental studies of the fundamental phenomena of nucleate boiling in microgravity. In particular, a better understanding of the complicated dynamics of bubble growth, coalescence, detachment, the effect of the flow, and bubble drift and accumulation in the stagnation areas is key for enabling successful designs. The proposed medium-scale on-orbit experiment concept is aimed at providing this vital information from a long-term microgravity environment of the ISS.

References

- [1] G. P. Sutton and O. Biblarz, *Rocket Propulsion Elements* (John Wiley and Sons, Inc., Hoboken, NJ, 2001).
- [2] D. J. Chato, *Cryogenics* **48**, 206 (2008).
- [3] D. Plachta and P. Kittel, *An Updated Zero Boil-Off Cryogenic Propellant Storage Analysis Applied to Upper Stages or Depots in an LEO Environment*, Tech. Rep. TM—2003-211691, NASA (2003).
- [4] B. F. Kutter, F. Zegler, G. O’Neil, and B. Pitchford, in *AIAA SPACE 2008 Conference and Exposition* (2008).
- [5] J. A. Goff, B. F. Kutter, F. Zegler, D. Bienhoff, F. Chandler, and J. Marchetta, in *AIAA SPACE 2009 Conference and Exposition* (2009).
- [6] S. M. Motil, M. L. Meyer, and S. P. Tucker, *Cryogenic Fluid Management Technologies for Advanced Green Propulsion Systems*, Tech. Rep. TM-2007-214810, NASA (2007).
- [7] L. J. Salerno and P. Kittel, *Cryogenics* **39**, 381 (1999).
- [8] R. F. Lacovic, F. C. Yeh, S. V. Szabo, R. J. Brun, A. J. Stofan, and J. A. Berns, *Management of cryogenic propellants in a full-scale orbiting space vehicle*, Tech. Rep. TN D-4571, NASA (1968).
- [9] D. Glover, *NASA Cryogenic Fluid Management Space Experiment Efforts 1960-1990*, Tech. Rep. TM-103752, NASA (1991).
- [10] F. T. Dodge, *The New “Dynamic Behavior of Liquids in Moving Containers”* (Southwest Research Institute, San Antonio, TX, 2000).
- [11] D. J. Chato, *Low gravity issues of cryogenic fluid management technologies enabling exploration* (2009).
- [12] M. P. Doherty, J. D. Gaby, L. J. Salerno, and S. G. Sutherlin, *Cryogenic Fluid Management Technology for Moon and Mars Missions*, Tech. Rep. TM-2010-216070, NASA (2010).
- [13] M. Donabedian, ed., *Spacecraft thermal control handbook. Volume 2, Cryogenics* (The Aerospace Press, El Segundo, CA, 2003).
- [14] D. J. Chato, *Cryogenics* **46**, 82 (2006).
- [15] NASA Technical Report HSM-R421-67, *Evaluation of AS-203 Low Gravity Orbital Experiment* (1967).
- [16] NASA-TM-X-881, *Apollo Systems Description. Volume II. Saturn Launch Vehicles* (1964).
- [17] V. K. Dhir, *J. Heat Transfer* **128**, 1 (2006).
- [18] E. I. Nesis, *Sov. Phys. – Uspekhi* **8**, 883 (1965).
- [19] C. E. Brennen, *Fundamentals of Multiphase Flows* (Cambridge University Press, 2005).
- [20] V. K. Dhir, in *Proceedings of 12th International Heat Transfer Conference*, Grenoble, France (2002).
- [21] J. Kim, *Jpn. Soc. Microgravity Appl.* **20**, 264 (2003).

- [22] NASA's *Exploration System Architecture Study (Final Report)*, NASA-TM-2005-214062 (2005).
- [23] E. M. Lifshits and L. P. Pitaevskii, *Course of Theoretical Physics*, vol. 8 (Pergamon Press, London, 1980).
- [24] NASA-TM-X-68725, *Apollo Program Summary Report* (1975).
- [25] NASA-TM-X-69534, *Saturn V Launch Vehicle Flight Evaluation Report – AS-512. Apollo 17 Mission* (1973).
- [26] R. W. Orloff, *Apollo by the Numbers: A Statistical Reference*, Tech. rep., NASA SP-2000-4029 (2000).
- [27] C. W. Keller, G. R. Cunningham, and A. P. Glassford, *Thermal performance of multilayer insulations*, Tech. Rep. CR-134477, NASA (1974).
- [28] J. R. Feller, *Some simple calculations to assess the effectiveness of passive and active boil-off reduction techniques to EDS*, NASA-ARC Cryogenics Group (2009).
- [29] L. Hastings, D. Plachta, L. Salerno, and P. Kittel, *Cryogenics* **41**, 833 (2002).
- [30] M. E. Moran, *Cryogenic Fluid Storage Technology Development: Recent and Planned Efforts at NASA*, Tech. Rep. TM—2009-215514, NASA (2009).
- [31] C. Panzarella, D. Plachta, and M. Kassemi, *Cryogenics* **44**, 475 (2004).
- [32] J. Feller, L. Salerno, A. Kashani, J. Maddocks, B. Helvenstein, G. Nellis, and Y. Gianchandani, in *The Proceedings of the 15th International Cryocooler Conference* (2008).
- [33] E. R. Canavan, R. F. Boyle, and S. Mustafi, in M. S. El-Genk, ed., *Space Technology and Applications International Forum–STAIF 2008* (AIP, 2008), vol. 969, pp. 733–740.
- [34] J. F. LeBar and E. C. Cady, in *AIAA 2006-7454* (2006).
- [35] K. R. Hanby, *Handbook on Materials for Superconducting Machinery* (Battelle Columbus Labs, Ohio Metals and Ceramics Information Center, Columbus, OH, 1974).
- [36] M. P. Malkov, *A reference on physics and engineering fundamentals of cryogenics (in Russian)* (Energomizdat, Moscow, 1985).
- [37] A. Woodcraft, *Cryogenics* **45**, 421 (2005).
- [38] R. McCarty, J. Hord, and H. Roder, *Selected properties of hydrogen (engineering design data)*, vol. 168 of *Natl. Bur. Stand. Monographs* (National Bureau of Standards, 1981).
- [39] L. Bewilogua, R. Knöner, and G. Wolf, *Cryogenics* **6**, 36 (1966).
- [40] Y. A. Kirichenko, K. V. Rusanov, and E. G. Tyurina, *Cryogenics* **23**, 209 (1983).
- [41] L. Bewilogua, R. Knöner, and H. Vinzelberg, *Cryogenics* **15**, 121 (1975).
- [42] F. P. Incopera and D. P. DeWitt, *Fundamentals of Heat and Mass Transfer* (John Wiley and Sons, Inc., New York, 2007).
- [43] J. R. Feller, D. W. Plachta, G. Mills, and C. McLean, *Demonstration of a Cryogenic Boil-Off Reduction System Employing an Actively Cooled Thermal Radiation Shield*, Tech. rep., NASA (2010).
- [44] R. H. Flachbart, L. J. Hastings, A. Hedayat, S. L. Nelson, and S. Tucker, in J. G. W. II, ed., *CP985, Advances in Cryogenic Engineering: Transactions of the Cryogenic Engineering Conference — CEC* (2008), vol. 53.
- [45] F. W. Schmidt, R. E. Henderson, and C. H. Wolgemuth, *Introduction to Thermal Sciences* (John Wiley and Sons, Inc., 1993).
- [46] V. L. Streeter, E. B. Wylie, and K. W. Bedford, *Fluid Mechanics* (McGraw-Hill, 1998).
- [47] C. B. Muratov, V. V. Osipov, and V. Smelyanskiy, *Issues of Long-Term Cryogenic Propellant Storage in Microgravity*, Tech. rep., NASA (2011).
- [48] W. B. Streett, R. E. Sonntag, and G. J. V. Wylen, *The Journal of Chemical Physics* **40**, 1390 (1964).
- [49] G. Cini-Castagnoli, A. Giardini-Guidoni, and F. P. Ricci, *Phys. Rev.* **123**, 404 (1961).
- [50] W. P. A. Hass, G. Seidel, and N. J. Poulis, *Physica* **26**, 834 (1960).
- [51] R. Clift, J. R. Grace, and M. E. Weber, *Bubbles, Drops, and Particles* (Academic Press, New York, 1978).
- [52] R. Marek and J. Straub, *Int. J. Heat Mass Transfer* **44**, 619 (2001).
- [53] M. Barthes, C. Reynard, R. Santini, and L. Tadrist, *Europhys. Lett.* **77**, 14001 (2007).

- [54] S. H. Ho and M. M. Rahman, *Cryogenics* **48**, 31 (2008).
- [55] G. M. Zlobintsev, V. V. Kozinets, B. A. Merisov, E. M. Ogneva, V. I. Sokolov, and A. V. Blinova, *Metal Sci. and Heat Treat.* **17**, 436 (1975).
- [56] J. Straub, in J. P. Hartnett, ed., *Advances in Heat Transfer* (Academic Press, San Diego, CA, 2001), vol. 35.
- [57] M.-C. Duluc, B. Stutz, and M. Lallemand, *Int. J. Heat Mass Transfer* **51**, 1738 (2008).
- [58] M. E. Bland, C. A. Bailey, and G. Davey, *Cryogenics* **13**, 651 (1973).
- [59] J. Li and G. P. Petersen, *Int. J. Heat Mass Transfer* **48**, 4316 (2005).
- [60] M. M. Hasan, C. S. Lin, R. H. Knoll, and M. D. Bentz, *Tank Pressure Control Experiment: Thermal Phenomena in Microgravity*, Tech. Rep. TP-3564, NASA (1996).
- [61] J. Kim, *Int. J. Multiphase Flow* **35**, 1067 (2009).
- [62] M. S. Plesset and S. A. Zwick, *J. Appl. Phys.* **25**, 493 (1954).
- [63] L. E. Scriven, *Chem. Eng. Sci.* **10**, 1 (1959).
- [64] W. B. Bald, *Cryogenics* **16**, 709 (1976).
- [65] S. Siedel, S. Cioulachtjian, and J. Bonjour, *Exp. Therm. Fluid. Sci.* **32**, 1504 (2008).
- [66] V. S. Nikolayev, D. A. Beysens, G. L. Lagier, and J. Hegseth, *International Journal of Heat and Mass Transfer* **44**, 3499 (2001).
- [67] V. Nikolayev, D. Beysens, Y. Garrabos, C. Lecoutre, and D. Chatain, *Microgravity Sci. Technol.* **18**, 34 (2006).
- [68] V. S. Nikolayev, *Phys. Fluids* **22**, 082105 (2010).
- [69] J. Kim, J. F. Benton, and D. Wisniewski, *Int. J. Heat Mass Transfer* **45**, 3919 (2002).
- [70] C. D. Henry and J. Kim, *Int. J. Heat Fluid Flow* **25**, 262 (2004).
- [71] U. Heat Transfer Lab, *Nucleate boiling in the low gravity environment of the KC-135 aircraft.* (2009), http://boiling.seas.ucla.edu/multimedia_gallery.htm.
- [72] V. V. Osipov and C. B. Muratov, *Appl. Phys. Lett.* **93**, 224105 (2008).
- [73] Y. A. Kirichenko, L. A. Slobozhanin, and N. S. Shcherbakova, *Cryogenics* **23**, 110 (1983).
- [74] A. Mukherjee and V. K. Dhir, *Journal of Heat Transfer* **126**, 1023 (2004).